Computation of Transfer Maps from Surface Data with Applications to Wigglers

Using Elliptical Cylinders

Chad Mitchell and Alex Dragt
University of Maryland

April 2006 Version

Abstract

Simulations indicate that the dynamic aperture of proposed ILC Damping Rings is dictated primarily by the nonlinear properties of their wiggler transfer maps. Wiggler transfer maps in turn depend sensitively on fringe -field and high -multipole effects. Th erefore it is important to have detailed magnetic field data including knowledge of high spatial derivatives. This talk describes how such information can be extracted reliably from 3 -dimensional field data on a grid as provided, for example, by various 3 -dimensional field codes available from Vector Fields. The key ingredient is the use of surface data and the smoothing property of the inverse Laplacian operator.

Objective

- To obtain an accurate representation of the wiggler field that is analytic and satisfies Maxwell equations exactly. We want a vector potential that is analytic and $\nabla \times \nabla \times A = 0$.

- Use boundary value (surface) data to find an accurate series representation of interior vector potential through order N in (x,y) deviations from design orbit.

$$A_x(x, y, z) = \sum_{l=1}^{L} a_l^x(z) P_l(x, y)$$

L=27 for N=6

- Use a Hamiltonian expressed as a series of homogeneous polynomials

$$K = -\sqrt{\frac{(p_t + q\phi)^2}{c^2} - (\vec{p}_\perp - q\vec{A}_\perp)^2} - qA_z = \sum_{s=1}^{S} h_s(z) K_s(x, p_x y, p_y, \tau, p_\tau)$$

S=923 for N=6

- We compute the design orbit and the transfer map about the design orbit to some order. We obtain a factorized symplectic map for single-particle orbits through the wiggler:

$$M = R_2 e^{:f_3:} e^{:f_4:} e^{:f_5:} e^{:f_6:} \ldots$$

Fitting Wiggler Data

▪Data on regular Cartesian grid

4.8cm in x, dx=0.4cm

2.6cm in y, dy=0.2cm

480cm in z, dz=0.2cm

▪Field components Bx, By, Bz in one quadrant given to a precision of 0.05G.

▪Place an imaginary elliptic cylinder between pole faces, extending beyond the ends of the magnet far enough that the field at the ends is effectively zero.

▪Fit data onto elliptic cylindrical surface using bicubic interpolation to obtain the normal component on the surface.

▪Compute the interior vector potential and all its desired derivatives from surface data.
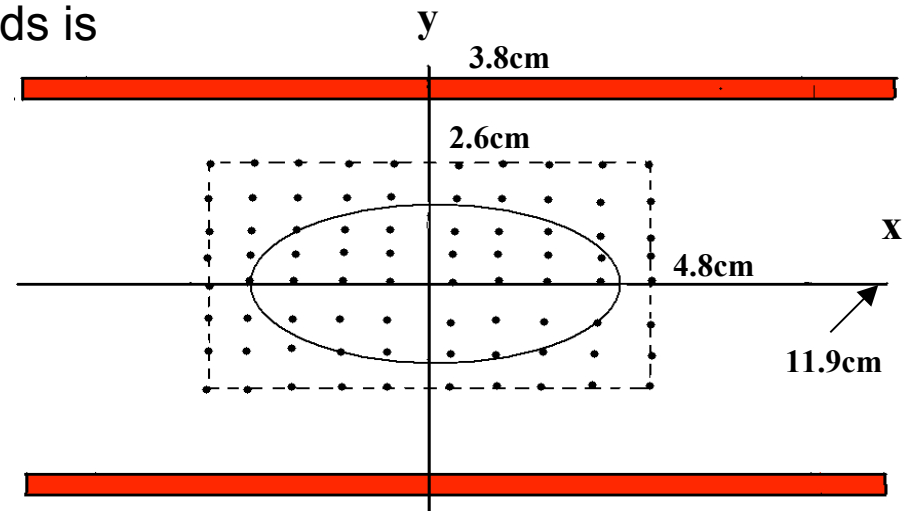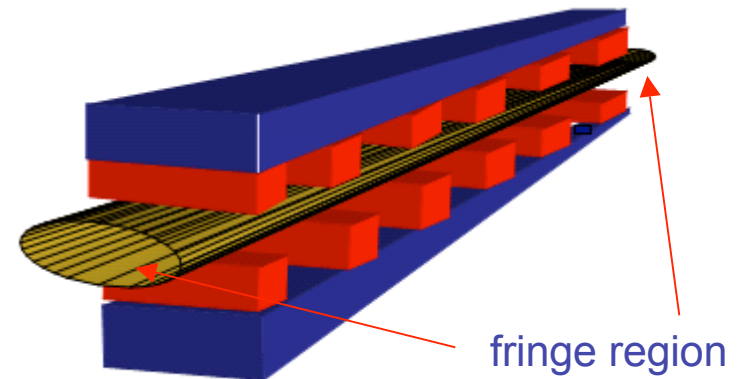
fringe region

Advantages of Surface Fitting

- Uses functions with known (orthonormal) completeness properties and known (optimal) convergence properties.

- Maxwell equations are exactly satisfied. (Other procedures.)

- Error is globally controlled. The error must take its extrema on the boundary, where we have done a controlled fit.

- Careful benchmarking against analytic results for arrays of magnetic monopoles.

- Insensitivity to errors due to inverse Laplace kernel smoothing. Improves accuracy in higher derivatives. Insensitivity to noise improves with increased distance from the surface: advantage over circular cylinder fitting.

Elliptic Coordinates

Defined by relations:

$$x = f \cosh u \cos v$$

$$y = f \sinh u \sin v$$

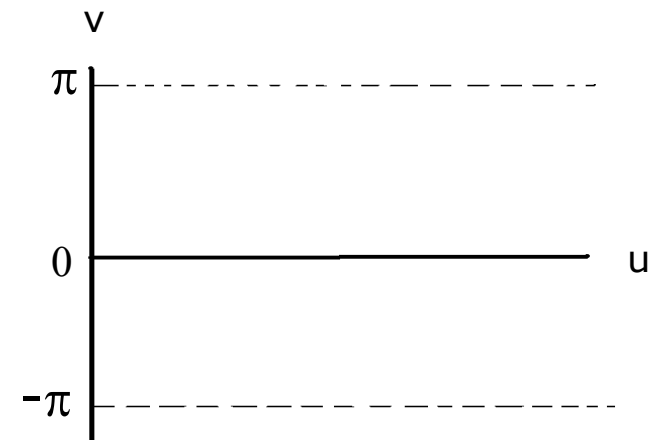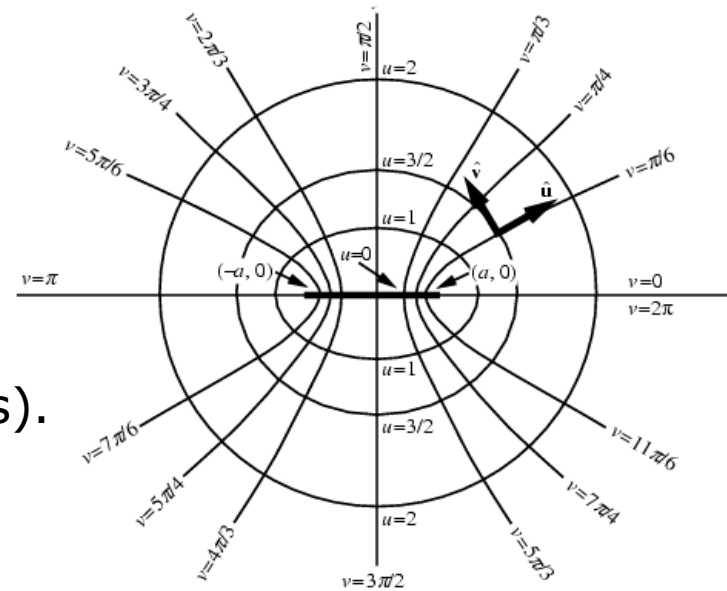where f=a (distance from origin to focus).

Letting z=x+iy, w=u+iv we have

$$z = \Im(w) = f \cosh w$$

Jacobian:

$$J(u,v) = \left|\Im'(w)\right|^2 = \left|f \sinh w\right|^2 = \frac{1}{2}f^2[\cosh(2u) - \cos(2v)]$$

Laplacian:

$$\nabla^2 = \frac{1}{J(u,v)}\left(\frac{\partial^2}{\partial u^2} + \frac{\partial}{\partial v^2}\right) + \frac{\partial^2}{\partial z^2}$$

- Fitting done in a source-free region, so we can use a scalar potential to write $\boldsymbol{B} = \nabla \psi$. Then $\nabla \cdot \boldsymbol{B} = 0$ gives the Laplace equation $\nabla^2 \psi = 0$. Make the Fourier decomposition

$$\psi(x,y,z) = \int_{-\infty}^{\infty} dk\, e^{ikz} \tilde{\psi}(x,y,k) \, ,$$

from which it follows that $(\nabla_{\perp}^2 - k^2)\tilde{\psi}(x,y,k) = 0$.

- Search for product solutions in elliptic coordinates $\tilde{\psi} \propto U(u)V(v)$

- Then we find that V and U satisfy the Mathieu Equations

$$\frac{d^2V}{dv^2} + \left[\lambda - 2q\cos(2v)\right]V = 0$$

$$\frac{d^2U}{du^2} - \left[\lambda - 2q\cosh(2u)\right]U = 0,$$

with $q = -\dfrac{k^2 f^2}{4}$.

- Periodicity in v forces $\lambda(q)$ to have certain characteristic values $\lambda = a_m(q)$ and $\lambda = b_m(q)$.

The solutions for V are

Mathieu functions

$$ce_m(v,q) \quad \longleftarrow \quad \text{even in } v$$

$$se_m(v,q) \quad \longleftarrow \quad \text{odd in } v$$

The associated solutions for U are

Modified Mathieu functions

$$Ce_m(u,q) = ce_m(iu,q),$$

$$Se_m(u,q) = -ise_m(iu,q).$$

By abuse of notation, we also write $se_m(v,k) = se_m(v,q(k))$, etc.

Boundary-Value Solution

Normal component of field on bounding surface defines a Neumann problem with interior field determined by angular Mathieu expansion on the boundary:

For $\tilde{\Psi}(x,y,k)$ we make the Ansatz

$$\tilde{\psi}(x,y,k) = \sum_{n=0}^{\infty}\left[\left(\frac{F_n(k)}{Se_n'(u_b,k)}\right)Se_n(u,k)se_n(v,k) + \left(\frac{G_n(k)}{Ce_n'(u_b,k)}\right)Ce_n(u,k)ce_n(v,k)\right].$$

where the functions $F_n(k)$ and $G_n(k)$ are yet to be determined, and u_b is the value of u on the surface.

We then find on the boundary surface the result

$$\sqrt{J(u_b,v)}\,\tilde{\boldsymbol{B}}_u(u_b,v,k) = \partial_u\tilde{\psi} = \sum_{n=0}^{\infty}F_n(k)se_n(v,k) + G_n(k)ce_n(v,k)$$

where the normal component of $\boldsymbol{B}$ on the surface is

$$\boldsymbol{B}_u(u_b,v,z) = \int_{-\infty}^{\infty}dke^{ikz}\,\tilde{\boldsymbol{B}}_u(u_b,v,k)$$

.

Using orthogonality properties of the se_m and ce_m gives for F_n and G_n the relations

$$F_m(k) = \int_0^{2\pi} dv \sqrt{J(u_b, v)}\, \tilde{B}_u(u_b, v, k)\, se_m(v, k)$$

$$G_m(k) = \int_0^{2\pi} dv \sqrt{J(u_b, v)}\, \tilde{B}_u(u_b, v, k)\, ce_m(v, k)$$

Thus, $\psi(x, y, z)$ is completely determined by the normal component of $\boldsymbol{B}$ on the surface of the elliptical cylinder.

Power Series Expansion in x and y

Various identities involving Mathieu functions and Bessel functions enable the expansion of $\psi(x,y,z)$ as a power series in x and y with z-dependent coefficients, and corresponding power series expansions of the vector potential A in the form:

$$A_{\left\{{x \atop y}\right\}} = \sum_{m=1}^{\infty}\sum_{l=0}^{\infty}\frac{(-1)^l(m-1)!}{2^{2l}\,l!(l+m)!}\left\{{x \atop y}\right\}(x^2+y^2)^l\left[\mathrm{Re}(x+iy)^m\,C_{m,s}^{[2l+1]}(z) - \mathrm{Im}(x+iy)^m\,C_{m,c}^{[2l+1]}(z)\right]$$

$$A_z = \sum_{m=1}^{\infty}\sum_{l=0}^{\infty}\frac{(-1)^l(2l+m)(m-1)!}{2^{2l}\,l!(l+m)!}(x^2+y^2)^l\left[-\mathrm{Re}(x+iy)^m\,C_{m,s}^{[2l]}(z) + \mathrm{Im}(x+iy)^m\,C_{m,c}^{[2l]}(z)\right]$$

where

$$C_{r,s}^{[m]}(z) = \frac{1}{\sqrt{2\pi}}\frac{i^m}{2^r\,r!}\int_{-\infty}^{\infty}dk\,e^{ikz}k^{r+m}\left[\sum_{n=0}^{\infty}\frac{g_s^{2n+1}(k)B_r^{(2n+1)}(k)}{Se'_{2n+1}(u_b,k)}F_{2n+1}(k)\right]$$

$$C_{r,c}^{[m]}(z) = \frac{1}{\sqrt{2\pi}}\frac{i^m}{2^r\,r!}\int_{-\infty}^{\infty}dk\,e^{ikz}k^{r+m}\left[\sum_{n=0}^{\infty}\frac{g_c^{2n+1}(k)A_r^{(2n+1)}(k)}{Ce'_{2n+1}(u_b,k)}G_{2n+1}(k)\right]$$

- The quantities $C_{r,s}^{[m]}(z)$ and $C_{r,c}^{[m]}(z)$ are called generalized on-axis gradients. Note that

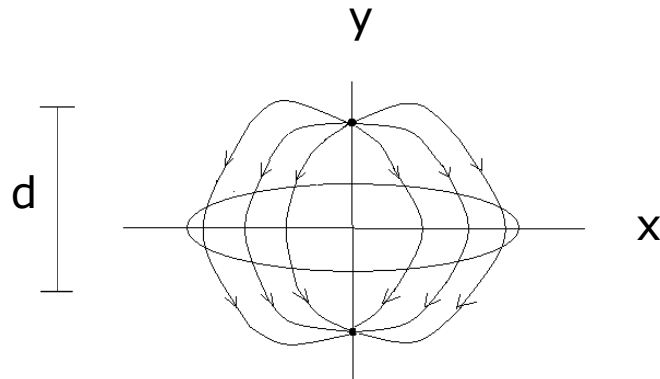$$C_{1,s}^{[2]} = \left(\frac{d}{dz}\right)^2 C_{1,s}, \text{ where } C_{1,s} = C_{1,s}^{[0]}, \text{ etc.}$$

- The vertical field then takes the form:

$$B_y = C_1(z) + 3C_3(z)(x^2 - y^2) - \frac{1}{8}C_1^{[2]}(z)(x^2 + 3y^2)$$

$$+ \frac{1}{192}C_1^{[4]}(z)(x^4 + 6x^2y^2 + 5y^4) - \frac{1}{16}C_3^{[2]}(z)(3x^4 + 6x^2y^2 - 5y^4)$$

$$+ C_5(z)(5x^4 - 30x^2y^2 + 5y^4) + O(x,y)^5$$

Here, for simplicity, we have assumed that $\mathbf{B}$ has midplane symmetry.

- There are similar expressions for the other components of $\mathbf{B}$ and the components of $\mathbf{A}$.

Dipole Field Test

- Simple field configuration in which scalar potential, field, elliptical moments, and on-axis gradients can be determined analytically.

- Tested for two different aspect ratios: 4:3 and 5:1.
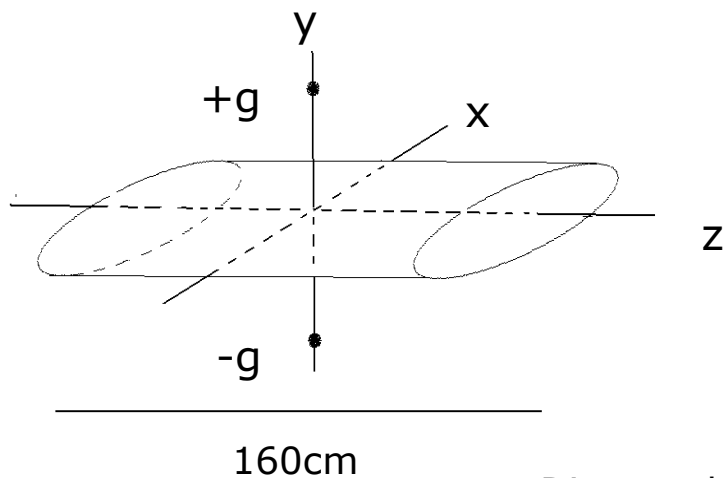
Pole location: d=4.7008cm

Pole strength: g=0.3Tcm^2

Semimajor axis: 1.543cm/4.0cm

Semiminor axis: 1.175cm/0.8cm

Boundary to pole: 3.526cm/3.9cm

Focal length: f=1.0cm/3.919cm

Bounding ellipse: u=1.0/0.2027

Direct solution for interior scalar potential
       accurate to 3*10-10: set by convergence/roundoff
Computation of on-axis gradients C1, C3, C5
       accurate to 2*10-10 before final Fourier transform
       accurate to 2.6*10-9 after final Fourier transform

Fit to the Proposed ILC Wiggler Field Using Elliptical Cylinder
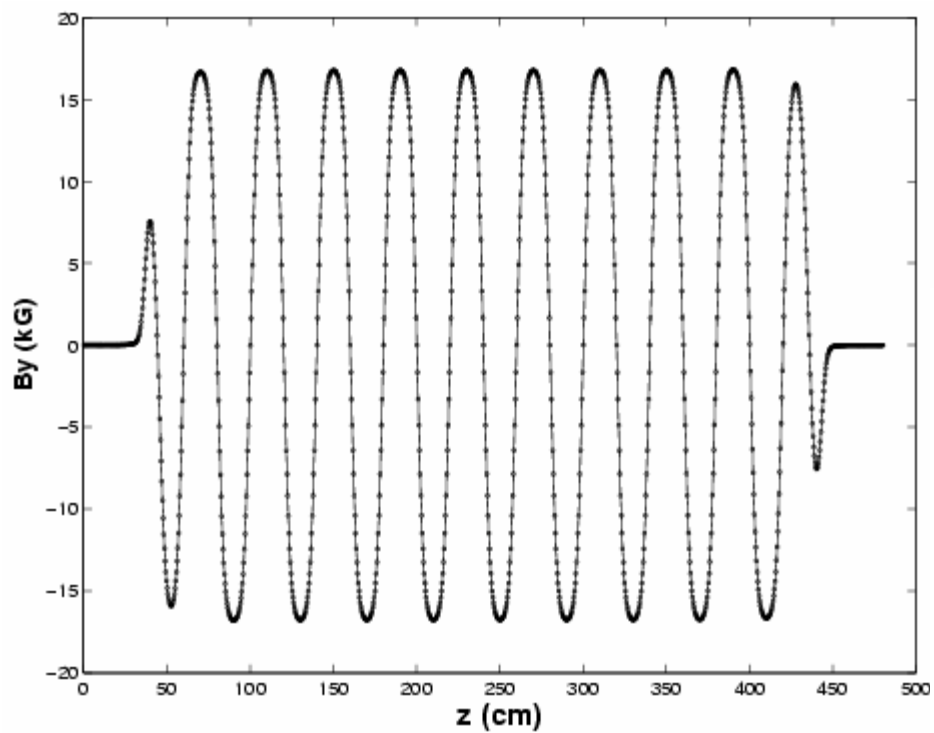
Fit to vertical field By
at x=0.4cm, y=0.2cm.

Note precision of data.
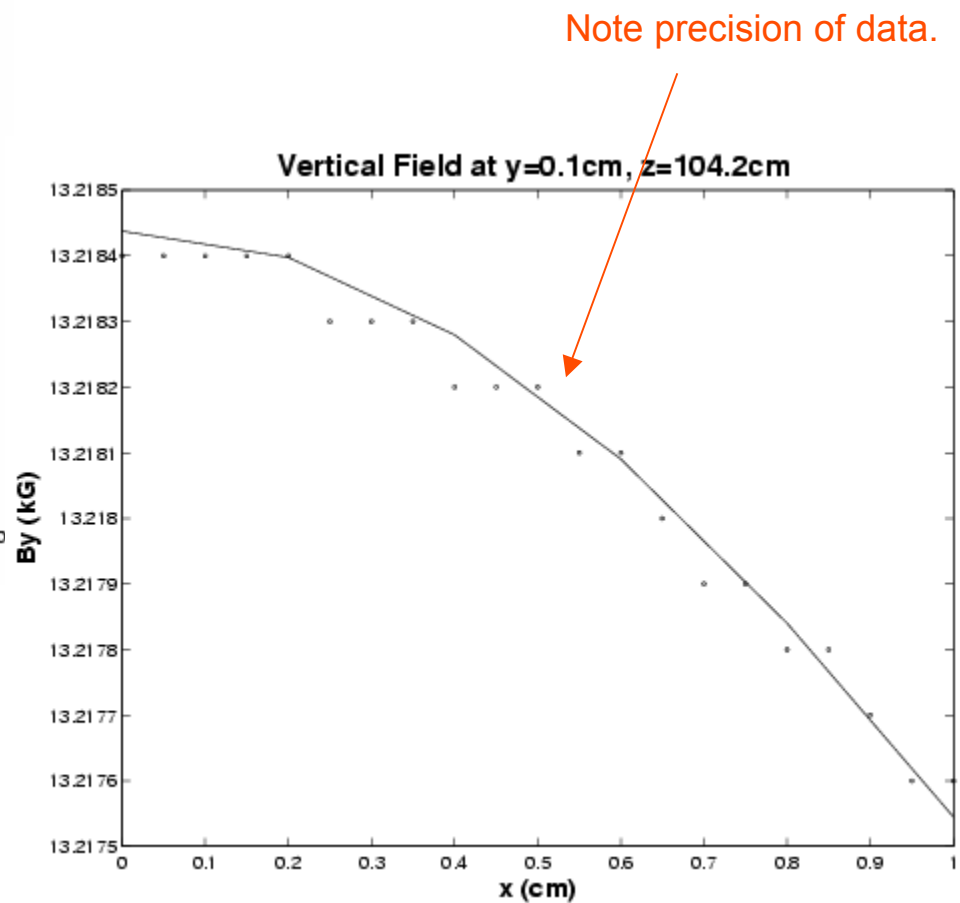
Fit to the Proposed ILC Wiggler Field Using Elliptical Cylinder

No information about Bz was used to create this plot.

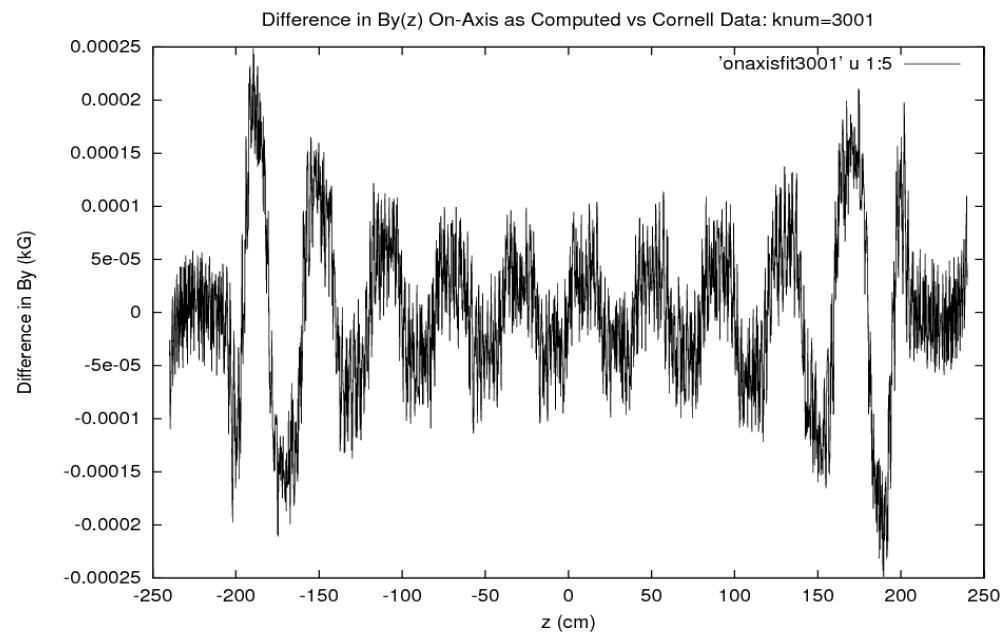Fit to longitudinal field Bz at x=0.4cm, y=0.2cm.

Fit to Longitudinal Field Bz(z) Using Elliptical Cylinder at (x,y)=(0.4,0.2) cm
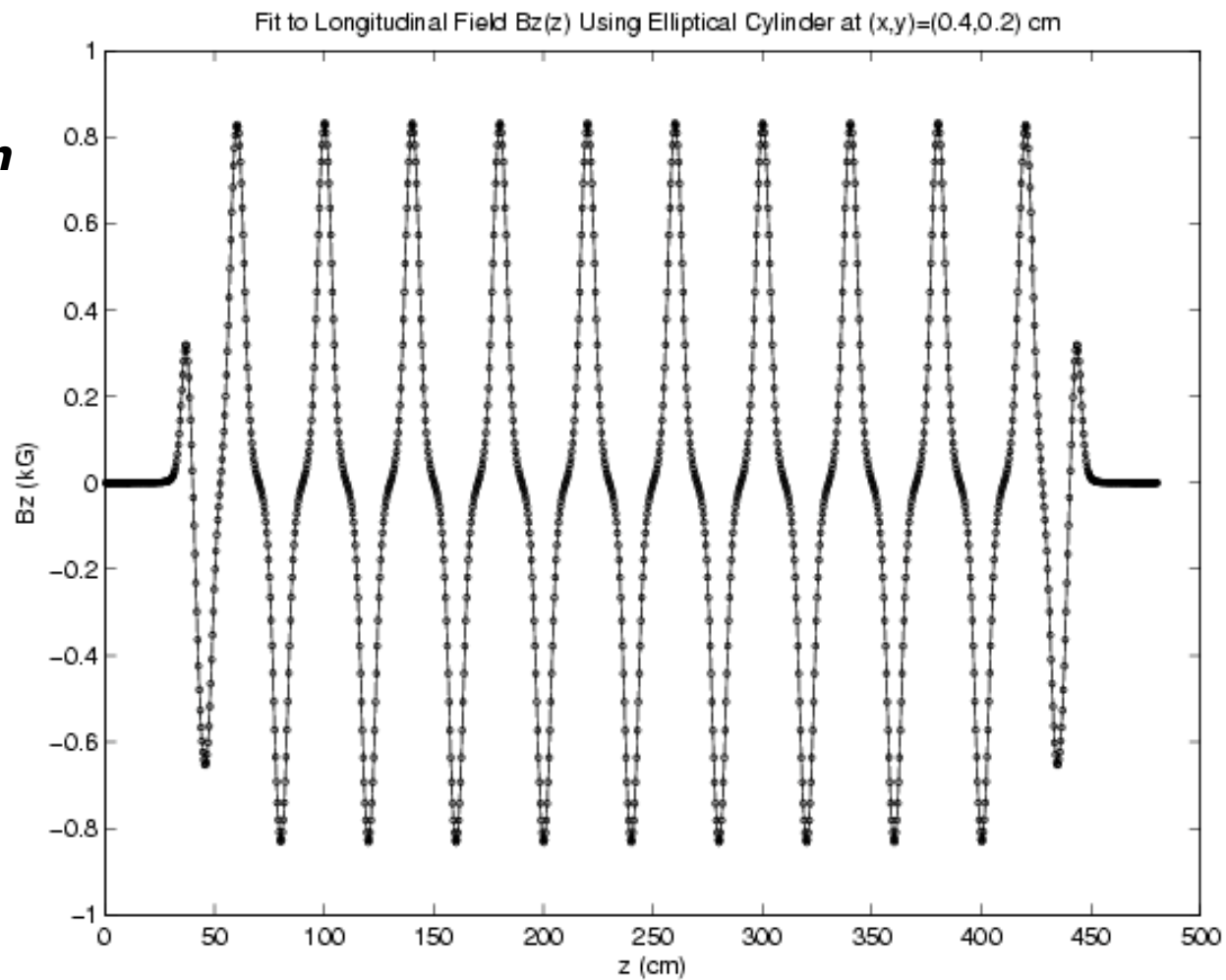
Residuals of fit to Cornell field data: field peaks near 17kG

Residual of fit to vertical field on plane y=0mm

'fieldmidplane' u ($1+240):2:($5*1000)

Difference in By (Gauss)

Difference in By(z) On-Axis as Computed vs Cornell Data: knum=3001

'onaxisfit3001' u 1:5 ———

Difference in By (kG)

z (cm)
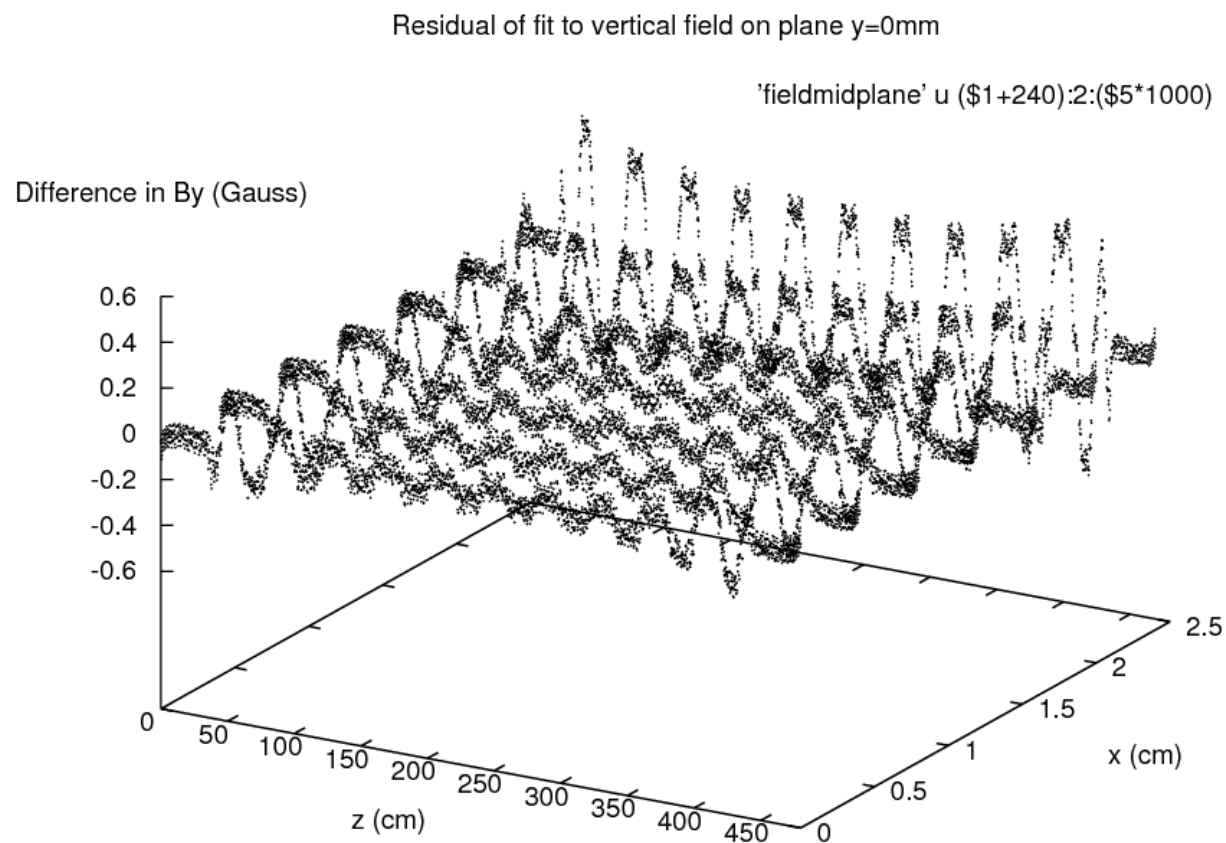
Residual of fit to vertical field on plane y=0mm over small-volume range

'smallvolmidplane' u ($1+240):2:($5*1000)   ·

Difference in By (Gauss)

x (cm)

z (cm)
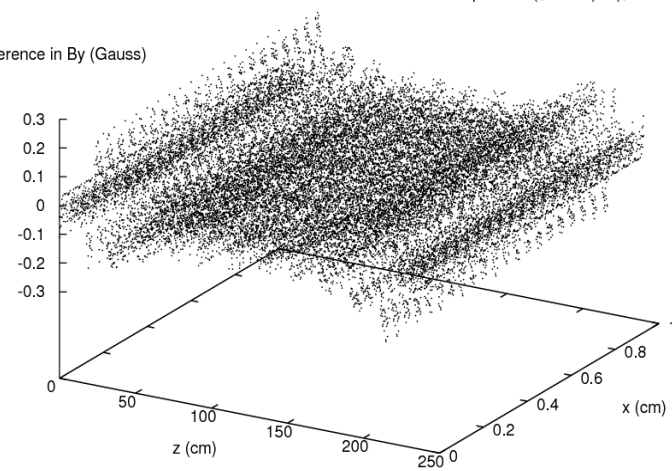
Reference orbit through proposed ILC wiggler at 5 GeV
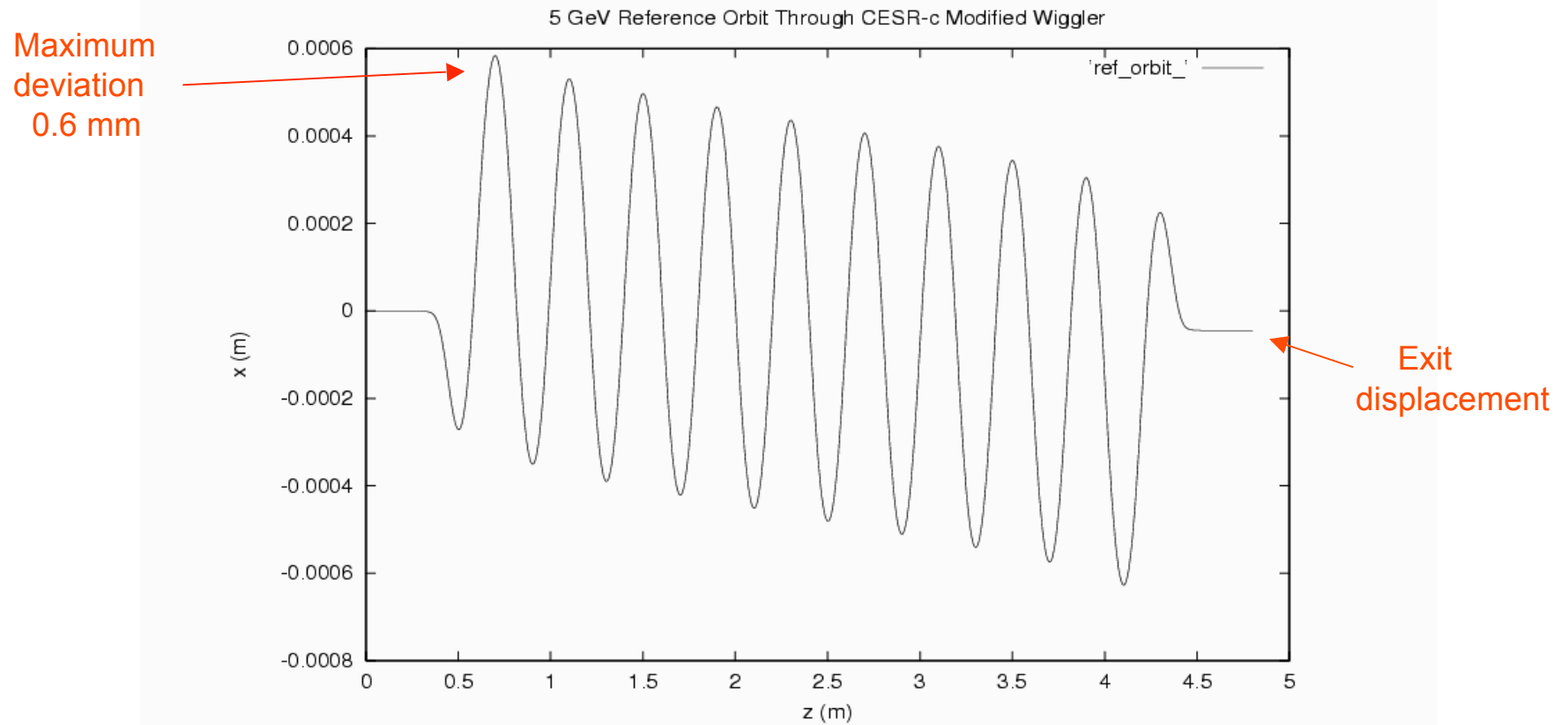
5 GeV Reference Orbit Through CESR−c Modified Wiggler

Phase space trajectory of 5 GeV on-axis reference particle

Phase Space Trajectory of 5 GeV On-Axis Reference Particle

'cesrref' u 2:3
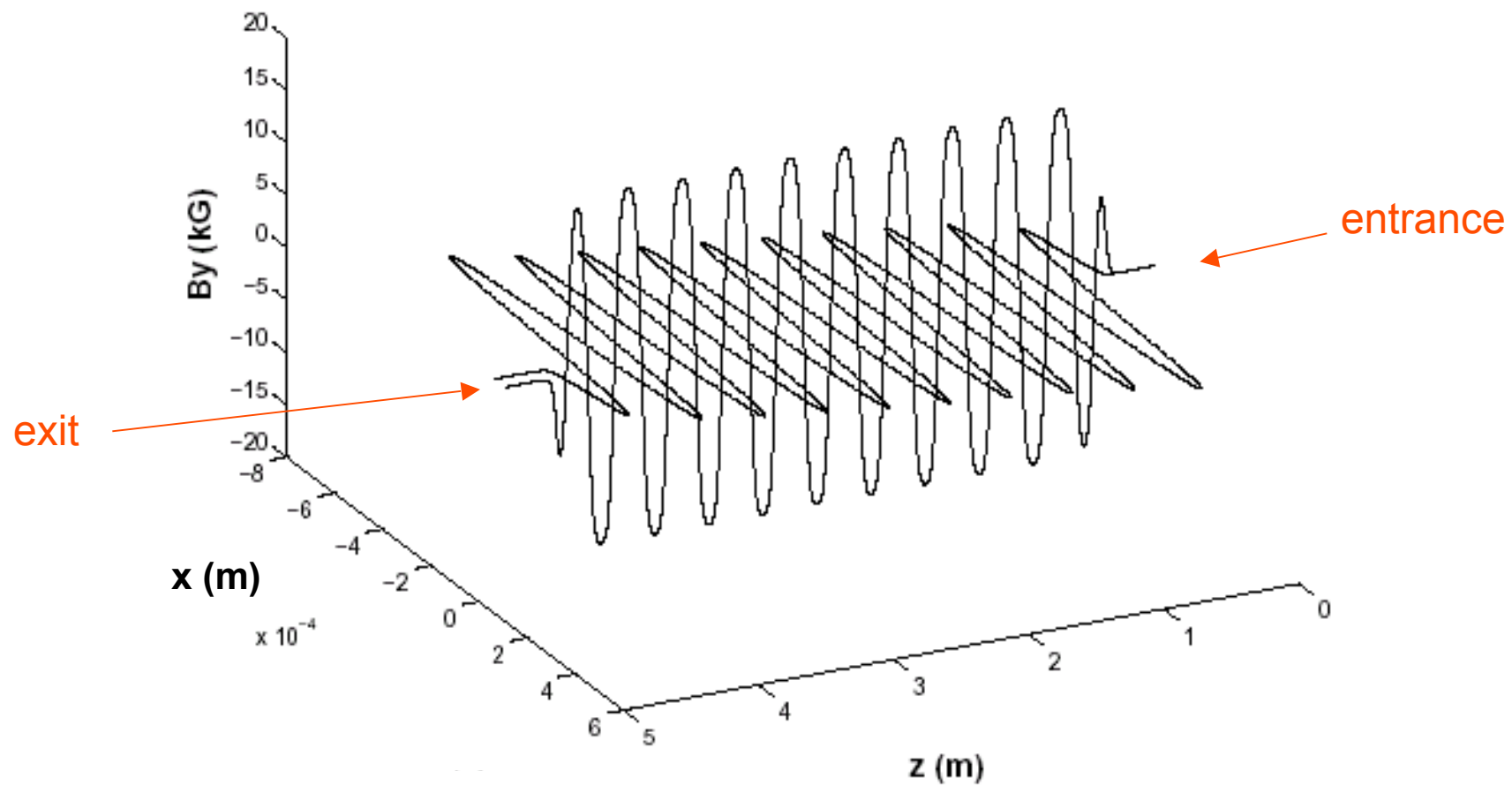
Mechanical momentum

px/p0

x (m)
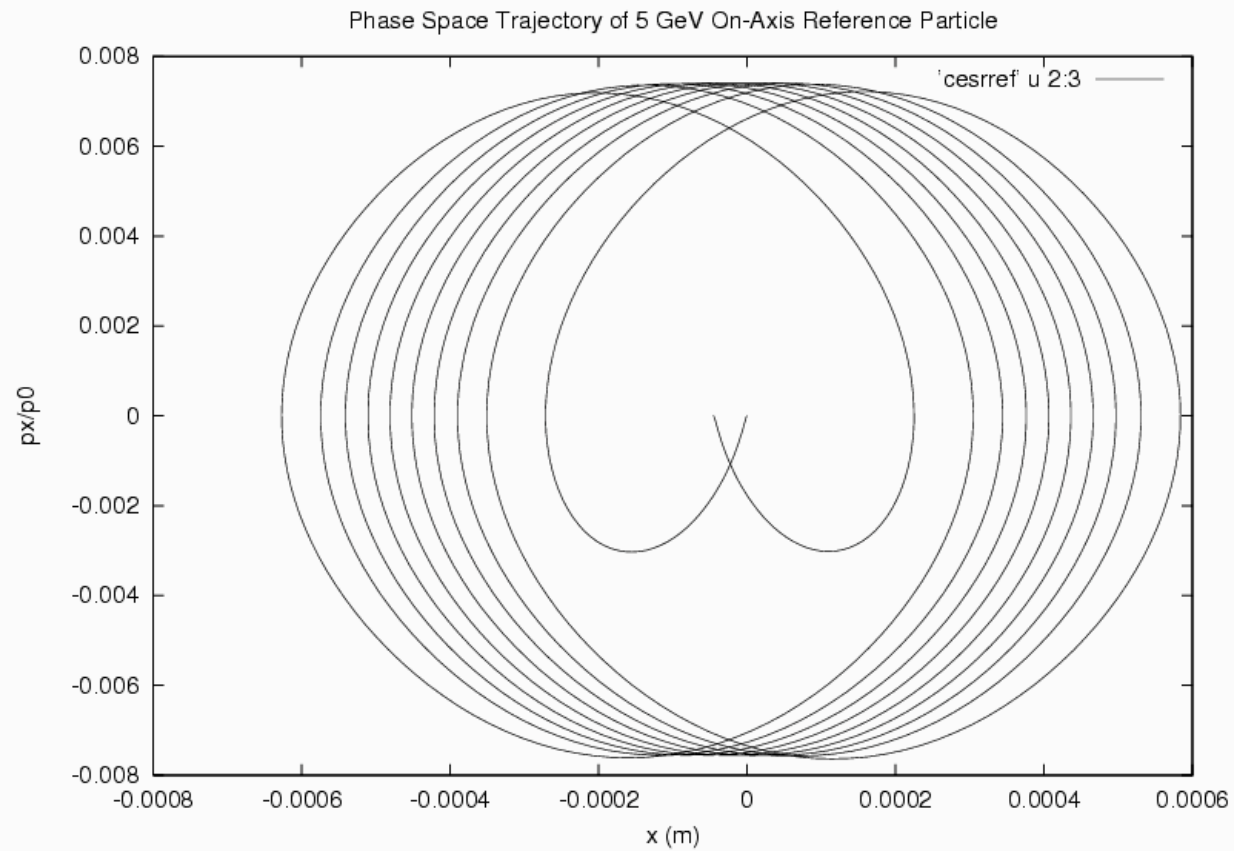
X (m)

REFERENCE ORBIT DATA

At entrance:

x (m) = 0.000000000000000E+000
can. momentum p_x = 0.000000000000000E+000
mech. momentum p_x = 0.000000000000000E+000
y (m) = 0.000000000000000E+000
mech. momentum p_y = 0.000000000000000E+000
angle phi_x (rad) = 0.000000000000000E+000
time (s) = 0.000000000000000E+000
p_t/(p0c) = -1.0000000052213336

At exit:

x (m) = -4.534523825505101E-005
can. momentum p_x   = 1.245592900543683E-007
mech. momentum p_x = 1.245592900543683E-007
y (m) = 0.000000000000000E+000
mech. momentum p_y = 0.000000000000000E+000
angle phi_x (rad) = 1.245592900543687E-007
time of flight (s) = 1.60112413288E-008
p_t/(p0c) = -1.0000000052213336

Bending angle (rad) = 1.245592900543687E-007

****

matrix for map is :

```
1.05726E+00  4.92276E+00   0.00000E+00   0.00000E+00  0.00000E+00 -5.43908E-05
2.73599E-02  1.07323E+00   0.00000E+00   0.00000E+00  0.00000E+00 -4.82684E-06
0.00000E+00  0.00000E+00   9.68425E-01   4.74837E+00  0.00000E+00  0.00000E+00
0.00000E+00  0.00000E+00  -1.14609E-02   9.76409E-01  0.00000E+00  0.00000E+00
3.61510E-06 -3.46126E-05   0.00000E+00   0.00000E+00  1.00000E+00  9.87868E-05
0.00000E+00  0.00000E+00   0.00000E+00   0.00000E+00  0.00000E+00  1.00000E+00
```

focusing

defocusing

nonzero elements in generating polynomial are :

f(28)=f(30 00 00)=-0.86042425633623D-03
f(29)=f(21 00 00)= 0.56419178301165D-01
f(33)=f(20 00 01)=-0.76045220664105D-03
f(34)=f(12 00 00)=-0.25635788141484D+00

. . . . Currently through f(923) – degree 6.

Theory of Smoothing

We have seen that the generalized on-axis gradients $C_r^{[m]}(z)$ are given as the Fourier integrals of the angular Mathieu coefficients F_{2n+1} and G_{2n+1} multiplied by certain kernels (weights). For example,

$$C_{r,s}^{[m]}(z) = \frac{1}{\sqrt{2\pi}} \frac{i^m}{2^r r!} \int_{-\infty}^{\infty} dk\, e^{ikz} k^{r+m} \left[\sum_{n=0}^{\infty} \frac{g_s^{2n+1}(k) B_r^{(2n+1)}(k)}{Se'_{2n+1}(u_b,k)} F_{2n+1}(k) \right]$$

$$\propto \int_{-\infty}^{\infty} dk\, e^{ikz} W_1^{r,m}(k) F_1(k) + \int_{-\infty}^{\infty} dk\, e^{ikz} W_3^{r,m}(k) F_3(k) + \dots$$

•Clean angular Mathieu coefficients (for the Cornell wiggler) cut off around k=2/cm. We expect noise to introduce high-frequency contributions to the spectrum of angular Mathieu coefficients $F_m(k)$.

•Kernels (weights) die off quickly for large k, providing an effective cutoff that serves as a low-pass filter to eliminate high-frequency components.

•Insensitivity to noise is improved by choosing geometry such that kernels approach zero quickly.

Wiggler Spectrum
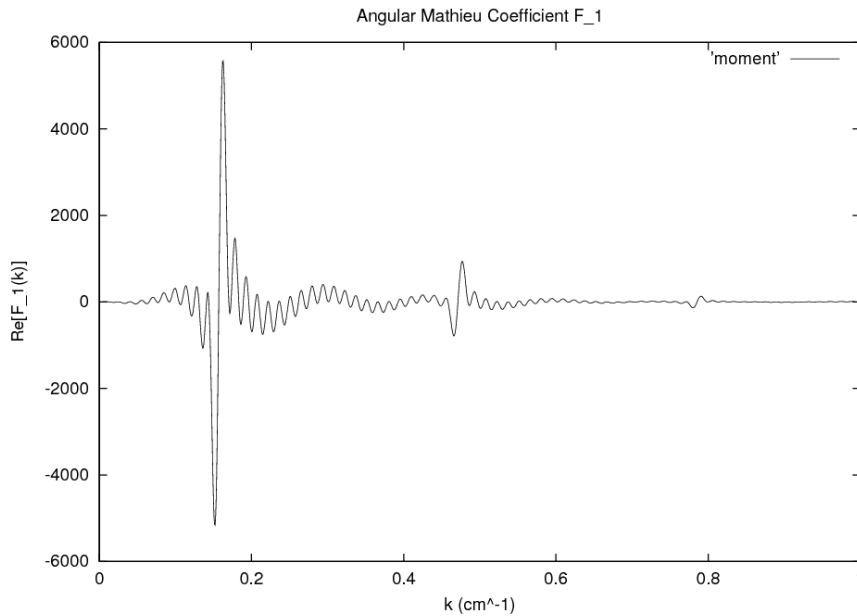
Angular Mathieu Coefficient F_1

Wiggler period: $L = 40cm$
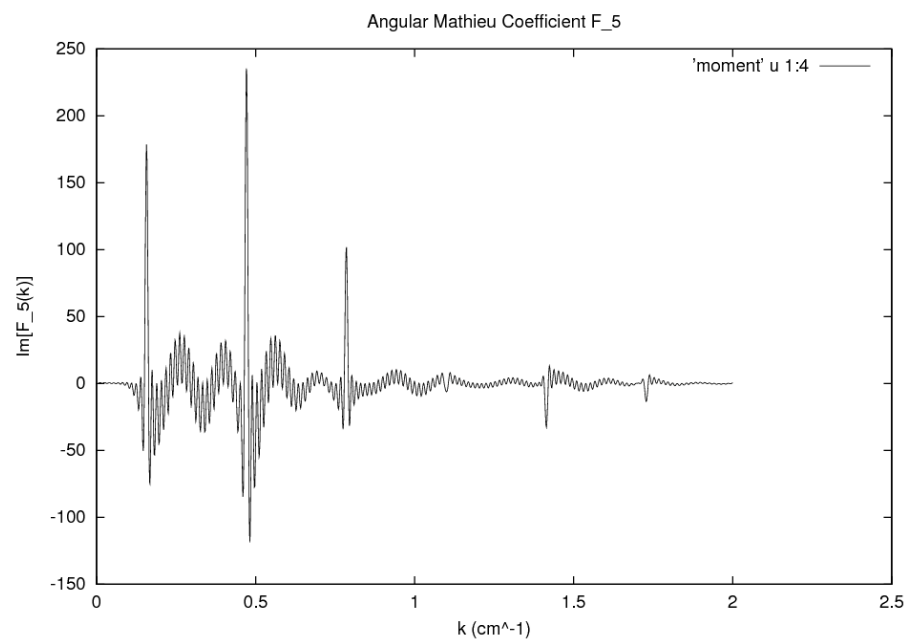
Peaks occur at frequencies corresponding to odd harmonics $k_n = 2\pi n / L = (0.1571n)cm^{-1}$

Amplitudes fall off by a factor of at least 0.1 for each harmonic; only the harmonics 1,3,5 contribute significantly.

Angular Mathieu coefficient F_1

Angular Mathieu Coefficient F_1
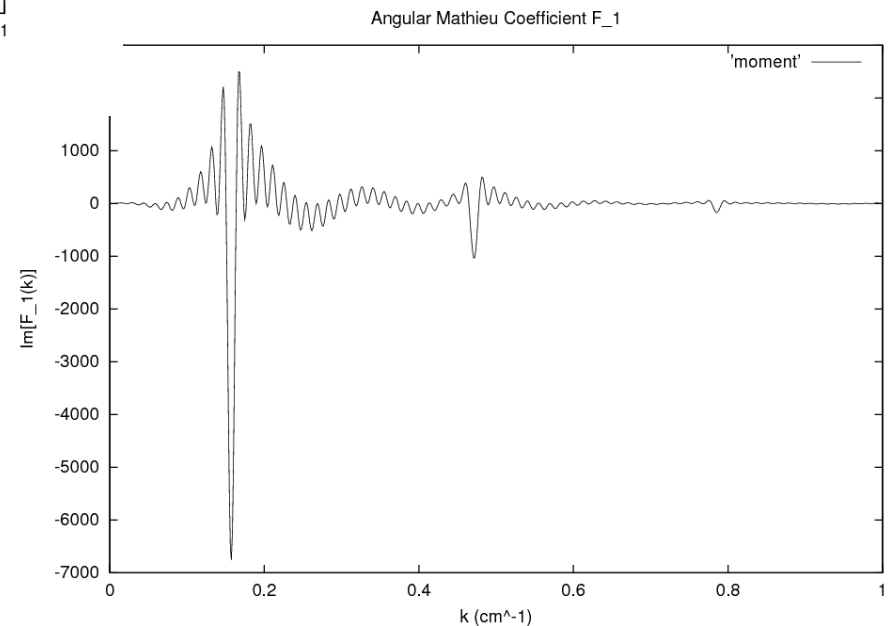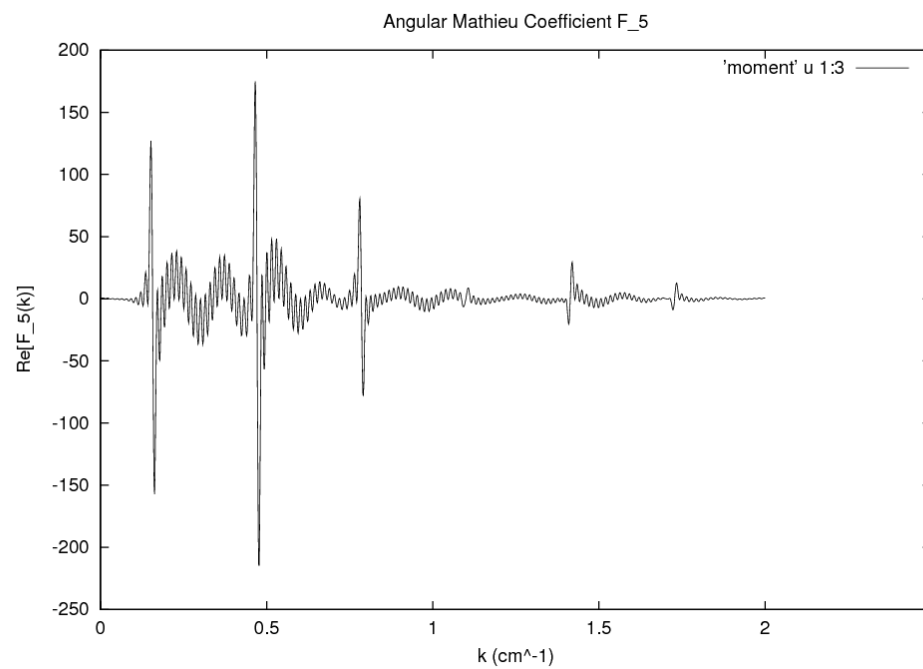
Angular Mathieu coefficient F_5

Weight Functions for an Elliptic Cylinder Boundary

▪Kernels W corresponding to the lowest 5 moments are plotted.

▪Note that these weight functions (kernels) cut off near k=4/cm, with cutoff increasing with order of kernel.

▪Nontrivial dependence on k.

Integration Kernels Corresponding to Lowest 6 Nonvanishing Moments for $C_3(z)$
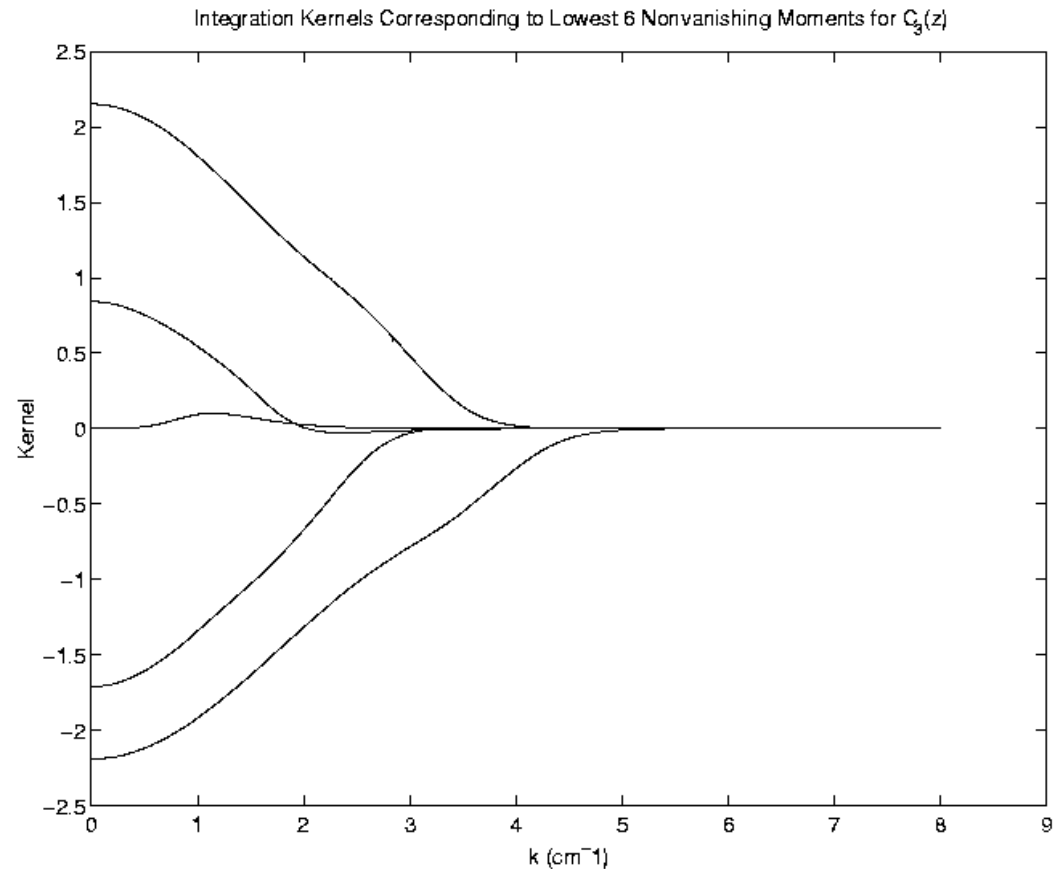
Comparison with Circular Case

There is one kernel for each gradient in the circular case. The kernels for $C_3(z)$ appear below. The circular kernel takes the form $k^2 / I'(kR)$ with R=1.

The first 4 elliptic kernels are shown for the case $y_{max}=1$, $x_{max}=4$.
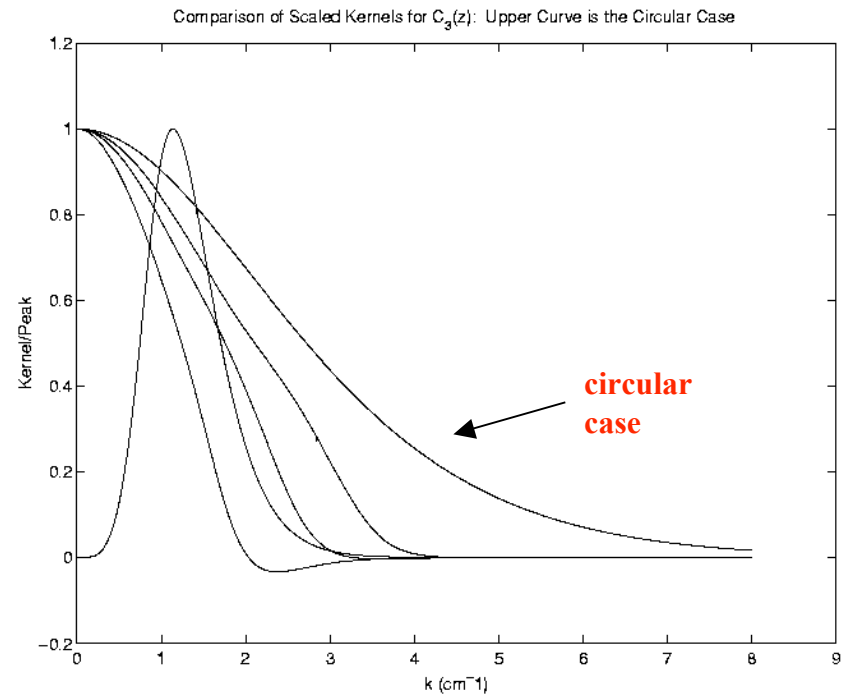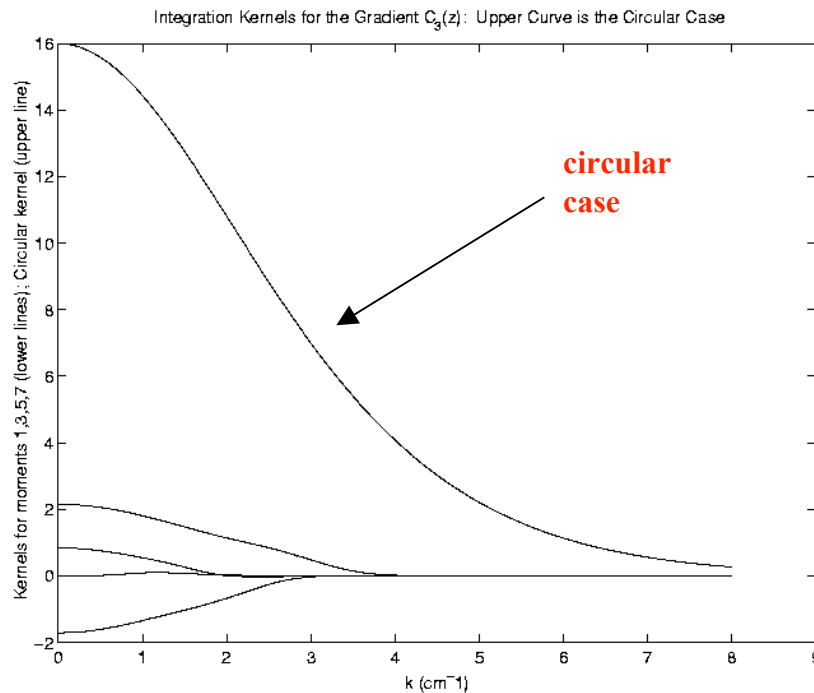
How Does Geometry Affect Smoothing Properties?

We expect accuracy to improve with enclosed cross-sectional area $\propto f^2 \sinh(2u_b)$
Interested in the following limiting behavior.

▪Simple Scaling – Fix aspect ratio $y_{max}/x_{max} = \tanh(u_b)$. Boundary scales linearly with f. How do the kernels behave for large focal distance f?
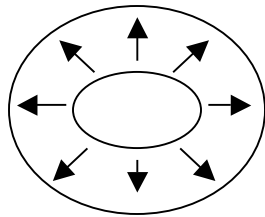
(No clean asymptotic form yet.)

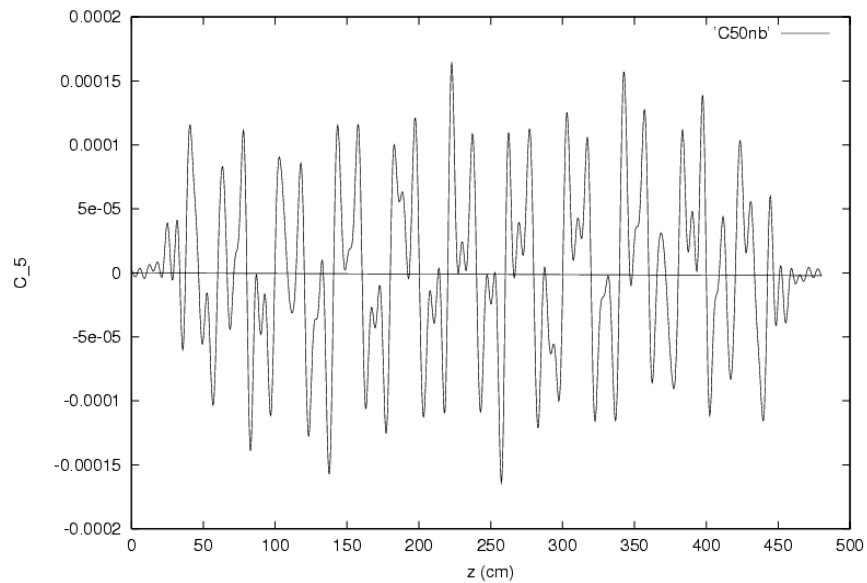▪Elongation – Fix semiminor axis y_{max}. What happens as the semimajor axis grows?
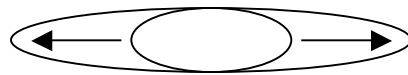
$$\propto k^{2r+2l+1}\sqrt{\pi k}\, B_{2r+1}^{(2n+1)}(k)\sqrt{\frac{y_{max}}{x_{max}}}\left(\frac{\sqrt{2}x_{max}}{y_{max}}\right)^{4n+4} e^{-kx_{max}}$$

▪Circular – Fix focal distance f. As u_b increases, this degenerates to the circular case.
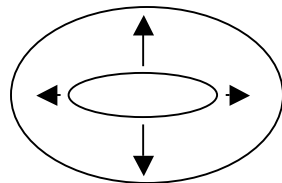
$$k^{2r+2l+1}\sqrt{\frac{2\pi}{kR}}e^{-kR}B_{2r+1}^{(2n+1)}(k)$$

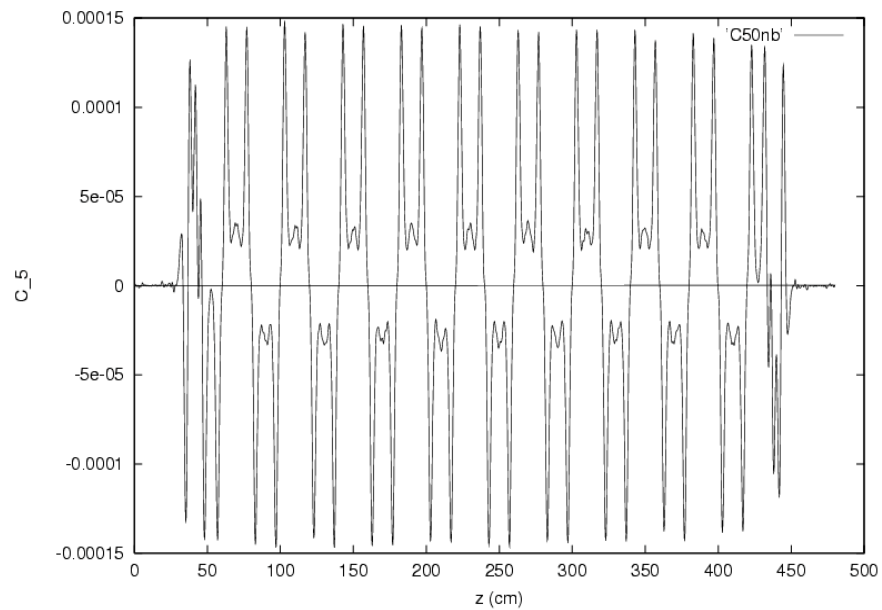## Gradient C_5(z) Computed Using 5/3 Aspect Ratio Domain

Effect of domain size on smoothing

(xmax,ymax)=(1,0.6)cm a.r.=5/3

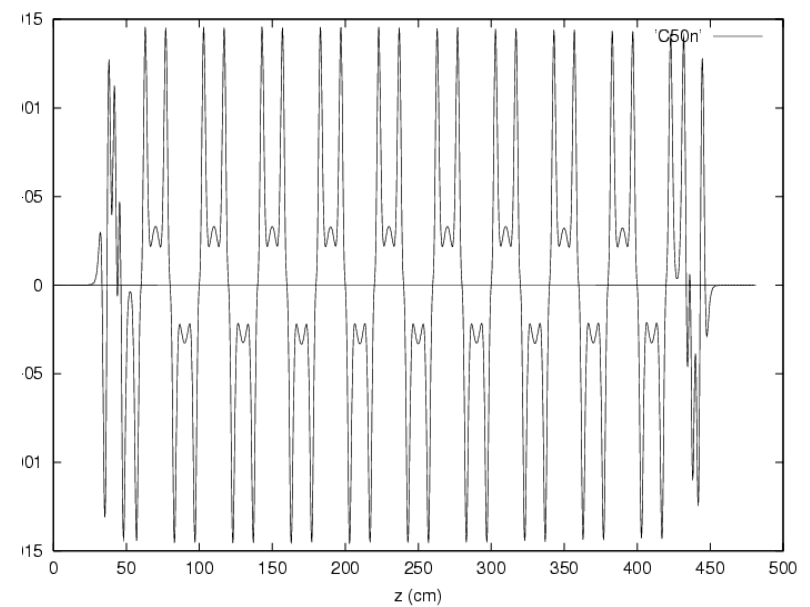(xmax,ymax)=(4.4,0.6)cm a.r.=22/3

(xmax,ymax)=(4.4,2.4)cm a.r.=11/6

Gradient C_5(z) Computed Using 22/3 Aspect Ratio Domain

Gradient C_5(z) Computed Using 11/6 Aspect Ratio Domain

Alternative Wiggler Field Fitting Technique

- A modified Fourier method for wiggler field fitting is written as:

$$\mathbf{B}_{fit} = \sum_{n=1}^{N} \mathbf{B}_n(x, y, s; C_n, k_{xn}, k_{sn}, \phi_{sn}, f_n)$$

where each term is written in one of three forms. For the present wiggler, each term is of the form:

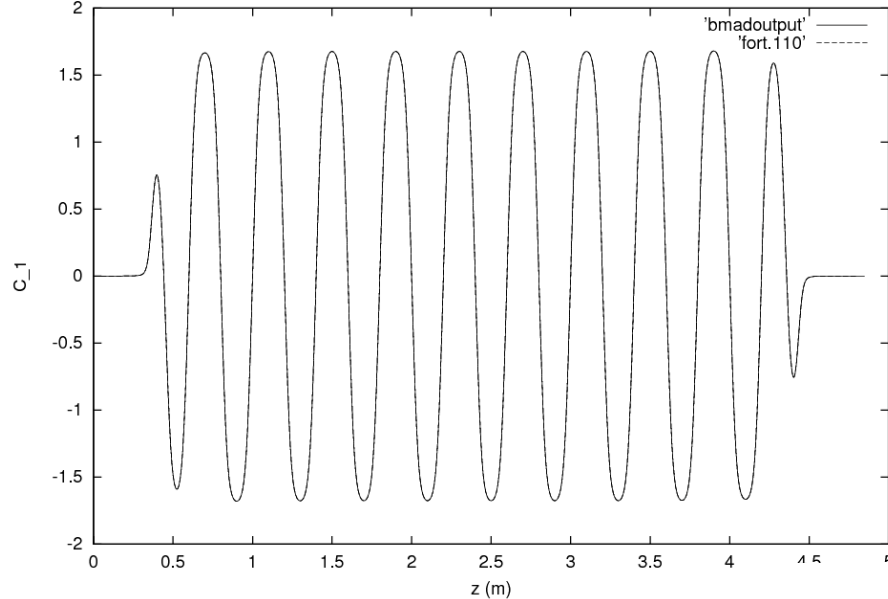$$B_x = -C\frac{k_x}{k_y}\sin(k_x x)\sinh(k_y y)\cos(k_s z + \phi_s)$$

$$B_y = C\cos(k_x x)\cosh(k_y y)\cos(k_s s + \phi_s) \qquad \text{with} \quad k_y^2 = k_x^2 + k_s^2$$

$$B_z = -C\frac{k_s}{k_y}\cos(k_x x)\sinh(k_y y)\sin(k_s s + \phi_s)$$

- The set of parameters $\{C_n, k_{xn}, k_{sn}, \phi_{sn} : n = 1,...,N\}$ is allowed to vary continuously, in such a way as to minimize the merit function:

$$M = \sum_{data\_pts}\left|\mathbf{B}_{fit} - \mathbf{B}_{data}\right|^2 + w_c\sum_{n=1}^{N}\left|C_n\right|$$
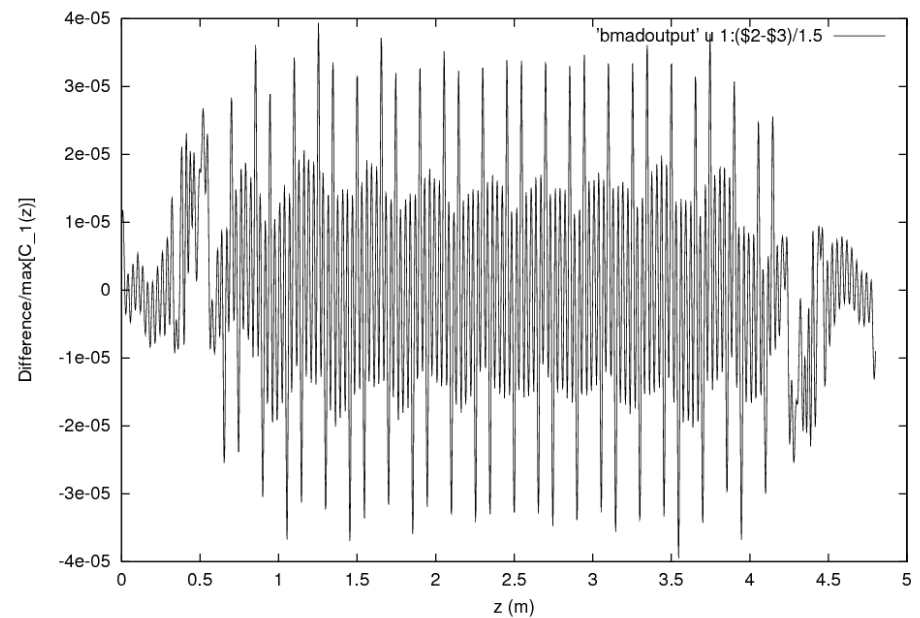
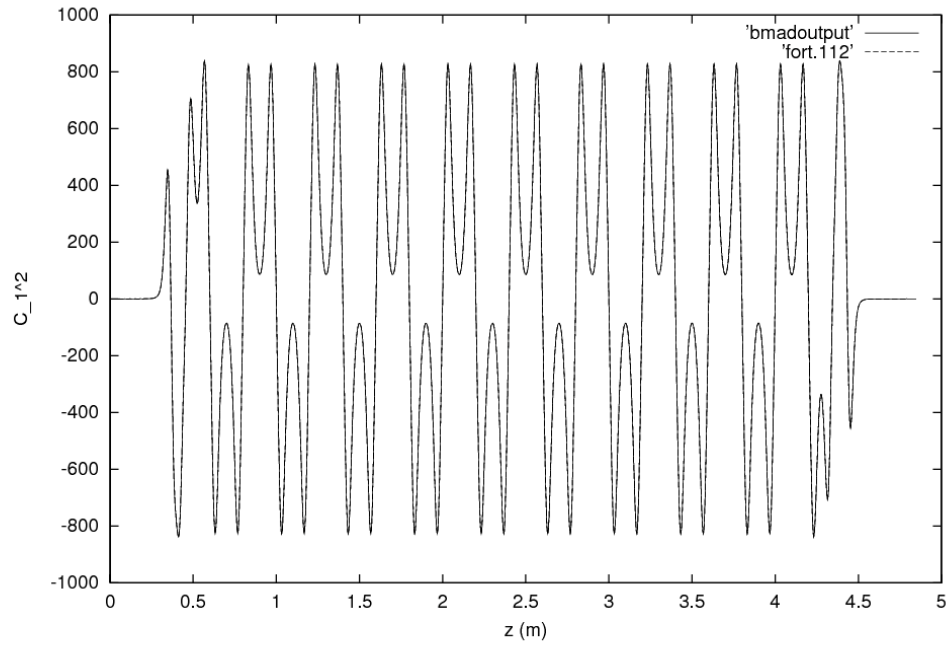**Comparison of Gradient C_1 Computed from Fourier Fit vs Boundary-Value Fit**

Comparison of on-axis gradient C_1 with the gradient obtained from Cornell's "Fourier" field fit

Solid line – Fourier field fit
Dashed line – Boundary-value fit

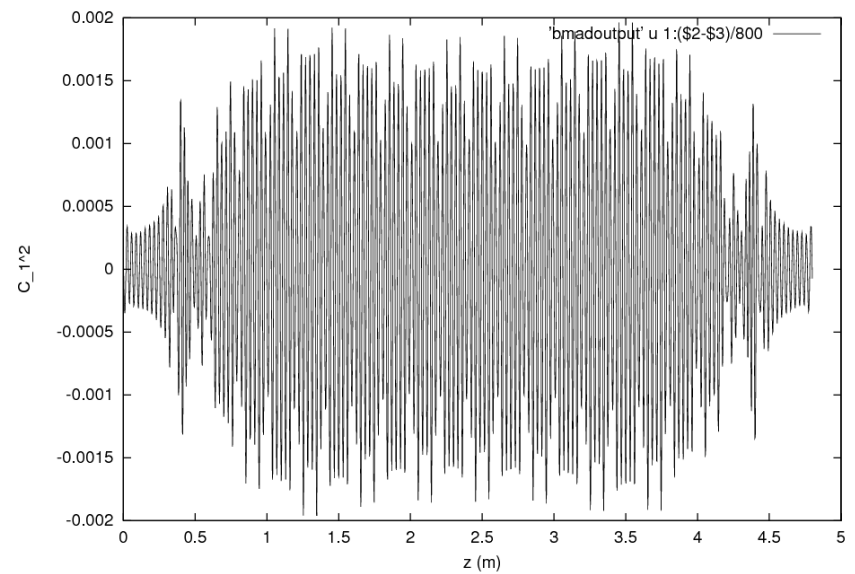**Difference Relative to Peak in Gradient C_1 Computed from Fourier Fit vs Boundary-Value Fit**

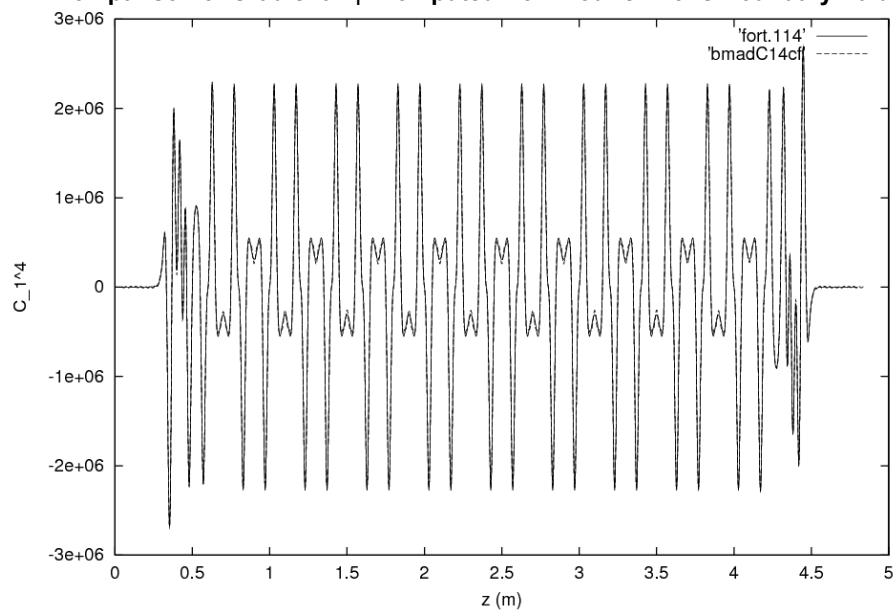**Comparison of Gradient $C_1{}^2$ Computed from Fourier Fit vs Boundary-Value Fit**

Comparison of on-axis gradient $C_1{}^{[2]}$ with the gradient obtained from "Fourier" field fit
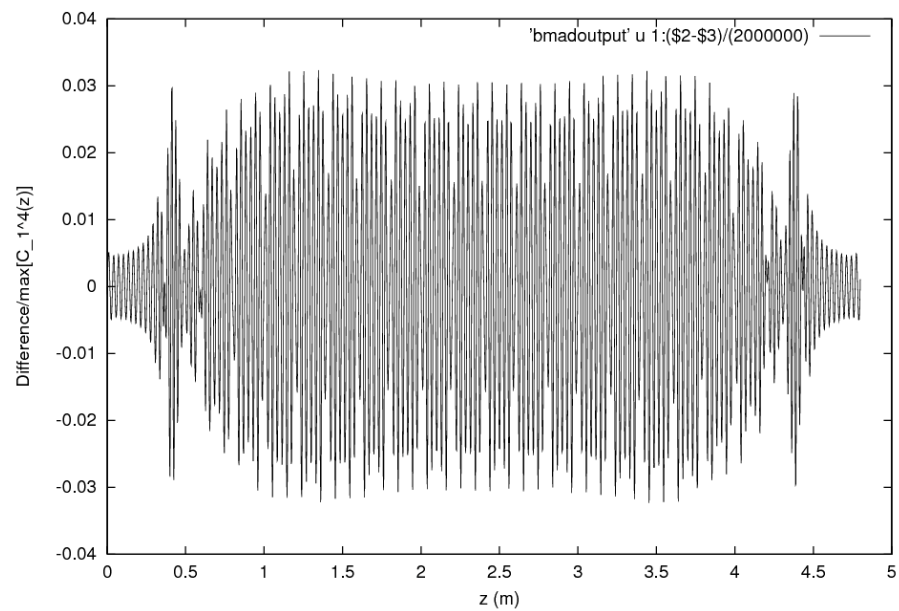
Difference Relative to Peak in Gradient $C_1{}^2$ Computed from Fourier Fit vs Boundary-Value Fit

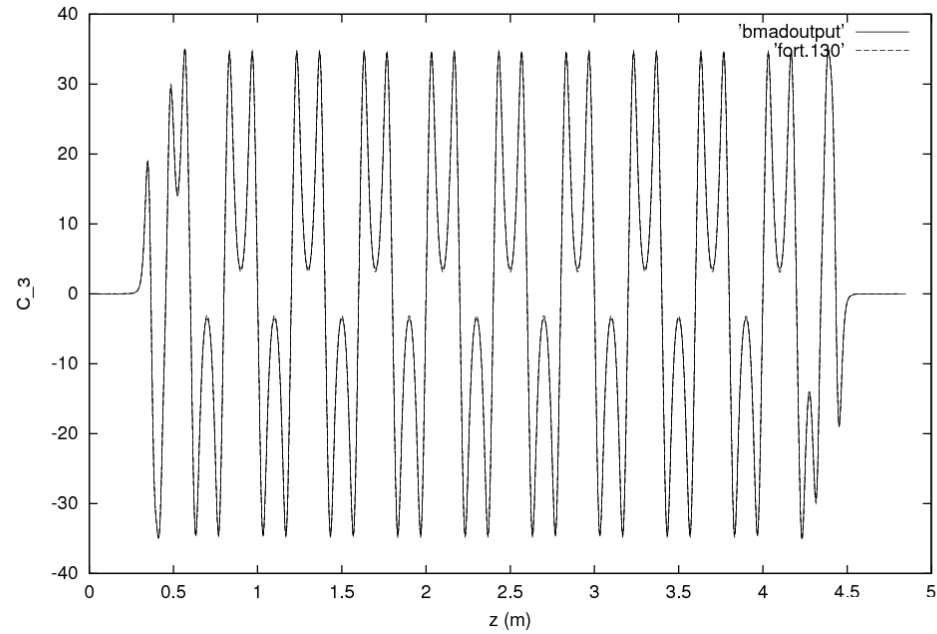## Comparison of Gradient C_1^4 Computed from Fourier Fit vs Boundary-Value Fit

Difference Relative to Peak in Gradient C_1^4 Computed from Fourier Fit vs Boundary-Value Fit
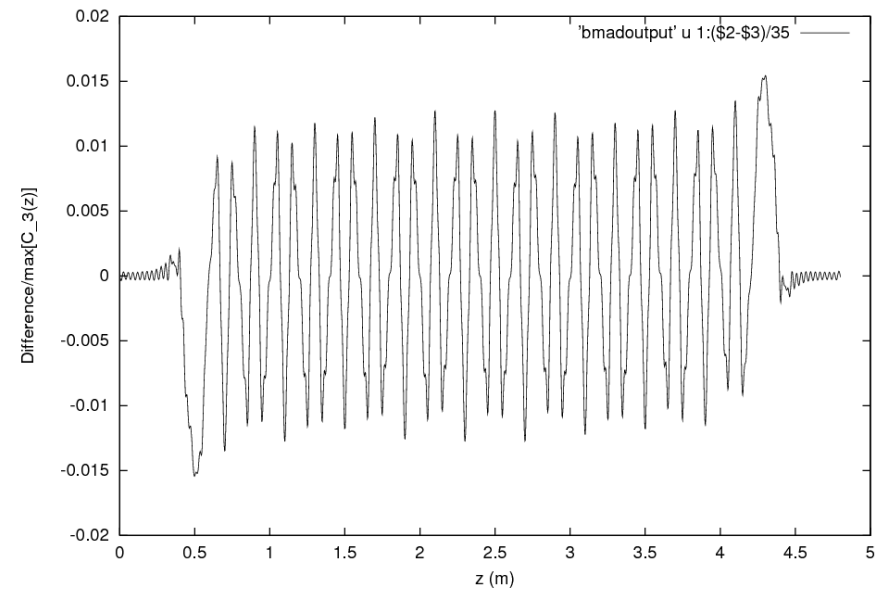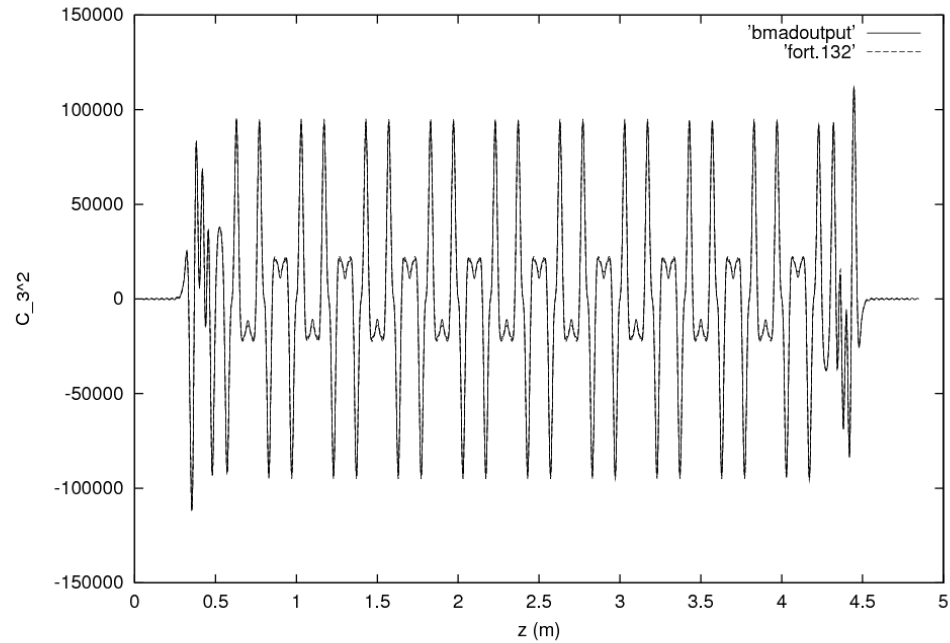
Comparison of Gradient C_3 Computed from Fourier Fit vs Boundary-Value Fit

Difference Relative to Peak in Gradient C_3 Computed from Fourier Fit vs Boundary-Value Fit

Comparison of Gradient C_3^2 Computed from Fourier Fit vs Boundary-Value Fit
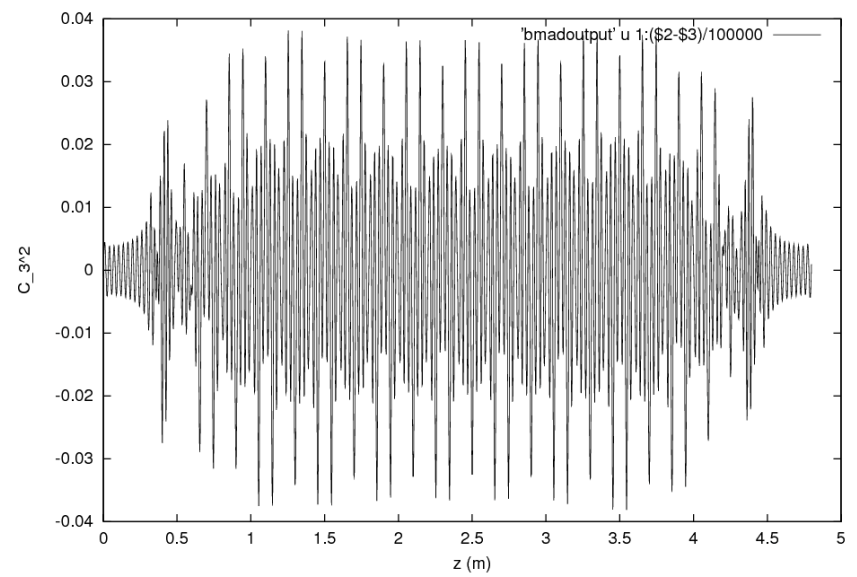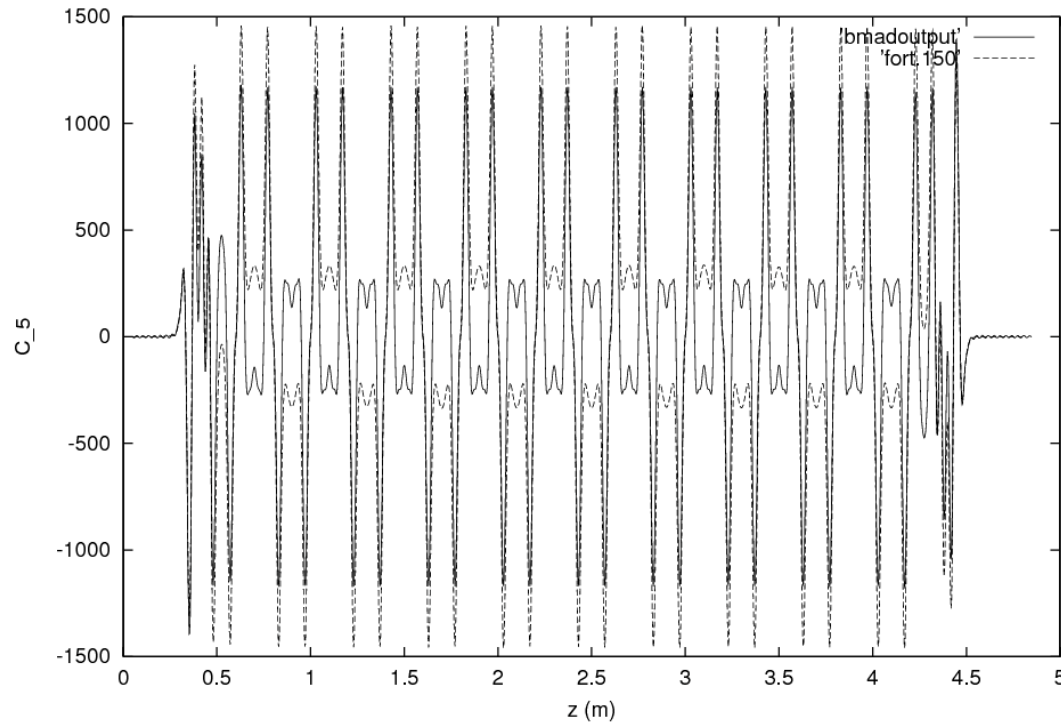
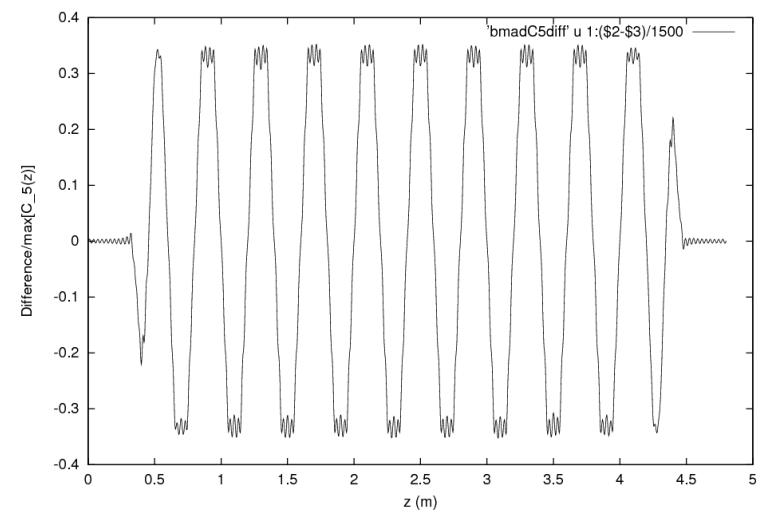**Difference Relative to Peak in Gradient C_3^2 Computed from Fourier Fit vs Boundary-Value Fit**

Comparison of Gradient C₅ Computed from Fourier Fit vs Boundary-Value Fit

Comparison of on-axis gradient C_5 with the gradient obtained from "Fourier" field fit

Difference Relative to Peak in Gradient C₅ Computed from Fourier Fit vs Boundary-Value Fit

Advantages of Surface Fitting

- Uses functions with known (orthonormal) completeness properties and known (optimal) convergence properties.

- Maxwell equations are exactly satisfied.

- Error is globally controlled. The error must take its extrema on the boundary, where we have done a controlled fit.

- Careful benchmarking against analytic results for arrays of magnetic monopoles.

- Insensitivity to errors due to inverse Laplace kernel smoothing. Improves accuracy in higher derivatives. Insensitivity to noise improves with increased distance from the surface: advantage over circular cylinder fitting.

Remarks about Geometry

- For the circular and elliptical cylinder, only the normal component of B on the surface was used to determine interior fields.

- The circular and elliptical cylinder are special in that Laplace's equation is separable for these domains.

- Laplace's equation is not separable for more general domains, e.g. a bent box.

- Surface data for general domains can again be used to fit interior data provided *both* Ψ and B_{normal} are available on the surface. Analogous smoothing behavior is again expected to occur.

The Bent Box and Other Geometries

The previous techniques can be used effectively for straight-axis magnetic elements.

For elements with significant sagitta, such as dipoles with large bending angles, we must generalize to more complicated domains in which Laplace's equation is not separable.

Given both ψ and B_{normal} on a surface enclosing the beam, the magnetic vector potential in the interior can be determined by the integration of surface data against a geometry-independent kernel.

$$A = A^n + A^t \quad \text{where}$$

$$A^n(r) = \frac{1}{4\pi} \oint_{S'} [n(r') \cdot B(r')] G^n(r;r',m(r')) dS'$$

$$A^t(r) = \frac{1}{4\pi} \oint_{S'} \psi(r') G^t(r;r',n(r')) dS'$$

We have the kernels:

$$G^n(r;r',m) = \frac{m \times (r - r')}{\left\{ \, |r - r'| - m \cdot (r - r') \, \right\} \, |r - r'|}$$

$$G^t(r;r',n(r')) = n(r') \times \nabla' \frac{1}{|r - r'|}$$

where m is a unit vector pointing along some line that does not intersect the interior (a Dirac string), and n is the unit normal to the surface at r'.

The kernels G^n and G^t are analytic in the interior. Given a point along the design orbit, we may construct a power series for A about r_d by integrating against the power series for the G's. Writing $\delta r = \delta x \hat{e}_x + \delta y \hat{e}_y$,

$$G(r_d + \delta r;r',n) = \sum_{\alpha=1}^{L} G_\alpha(r_d;r',n) P_\alpha(\delta x, \delta y)$$

This has been implemented numerically.

Implementation

The values of ψ and B_{normal} are again interpolated onto the boundary surface using polynomial splines.

torus

"bent box"
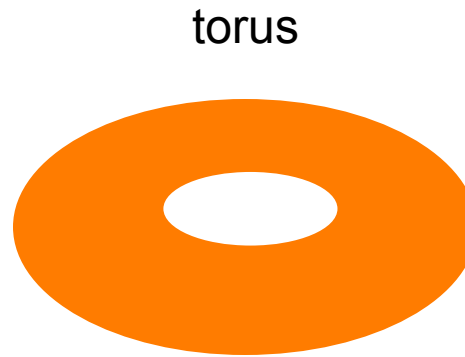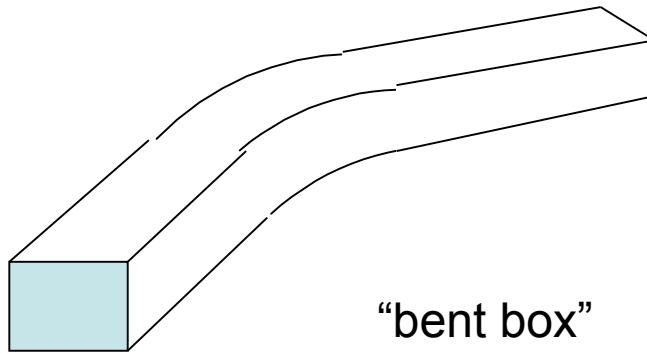
The procedure has been benchmarked for the above domains using arrays of magnetic monopoles to produce test fields. Power series for the components of B at a given point r_d are computed from the power series for A. These results can be compared to the known Taylor coefficients of the field. We find, using a surface fit that is accurate to 10^{-4}, that all computed coefficients are accurate to 10^{-6}.

Similarly, we verify that $\nabla \cdot B = 0$ and $\nabla \times B = 0$ to machine precision.

Box Fit to Wiggler Field

As an additional test, data provided by Cornell of the form (B_z, B_x, B_y, ψ) at grid points was fit onto the surface of a nearly-straight box filling the domain covered by the data.

Using this surface data, the power series for the vector potential was computed about several points in the interior. From this, the value of $\boldsymbol{B}$ was computed and compared to the initial data.

$$\boldsymbol{r}_d$$

Difference	(0.4, 0.2, 31.2)	(2, 2, 1)	(0, 1.4, 31.2)
Bx (G)	0.0417	0.187	0.230
By (G)	0.299	2.527	0.054
Bz (G)	0.161	0.626	0.916

Largest error/peak ~ 10^{-4}